

Internal Kinematics of the Seyfert Galaxy Mkn 938

V. L. Afanasiev, A. V. Moiseev and A. A. Smirnova

Special Astrophysical Observatory, Russian Academy of Sciences, Nizhnij Arkhyz, 369167 Russia

September 24, 2019/Revised: November 14, 2019

Abstract. We present the results of a detailed study of the central part of the Seyfert galaxy Mkn 938. Observational data were obtained with the 6-m telescope of the Special Astrophysical Observatory of the Russian Academy of Sciences using integral-field spectrograph MPFS and a scanning Fabry–Perot interferometer. Mkn 938 is interesting for being a result of a merger of two gas-rich galaxies, and we observe the final stage of this interaction accompanied with an extremely powerful burst of star formation and nuclear activity. Our analysis of the kinematics of gas and stars revealed the presence of gas outflow in the circumnuclear region Mkn 938 with velocities ranging from -370 to -480 km s^{-1} , and allowed us for the first time to map the high-velocity galactic wind in NaD absorption line on large spatial scale in this galaxy.

Key words. methods: observational—techniques: photometric—galaxies: active

1. INTRODUCTION

Studies of merging gas-rich galaxies provide an insight into the role that the dissipative processes along with gravitational processes play in the evolution of galaxies and galaxy systems (Schweizer & Seitzer, 2007). In recent decades great progress has been achieved in the understanding of the general role of mergers in the formation of early-type galaxies, and it is now generally believed that many of them are products of mergers of gas-rich galaxies. It is, however, not entirely clear how a gas-rich system eventually gets rid of gas and how this process is affected by a burst of star formation at the center and the presence of active nucleus. Bright star-forming regions and outflows form various components along the line-of-sight, which cannot be resolved in the sky plane. The application of the methods of two-dimensional (often referred to as 3D or integral-field) spectroscopy makes it possible to study such objects in detail. In this paper we report the results of 3D spectroscopy of the central part of the Mkn 938 galaxy. The main parameters of Mkn 938 are summarized in Table 1.

We classified the interacting galaxy Mkn 938 (= NGC 34 = VV 850), which has a peculiar morphology and active nucleus, as Sy 2 (Afanasiev et al., 1980). This classification was later confirmed (Dahari, 1985; Veron-Cetty & Veron, 1986). On the contrary, Osterbrock & Dahari (1983) classified it as emission-line galaxy dominated by star-forming regions, and Mulchaey et al. (1996) observed the galaxy

Table 1. The summary of Mkn 938

Activity type	Sy 2
Morphological type (NED)	Pec
Systemic velocity (Rothberg & Joseph, 2006)	5881 km s^{-1}
Adopted distance	85.2 Mpc
Image scale	395 pc/''
M_V (Schweizer & Seitzer, 2007)	-21.42
HI mass (Kandalyan, 2003)	$5.3 \times 10^9 M_\odot$
Maximum rotation velocity (our measurements for $i = 38^\circ$)	$225 \pm 6 \text{ km s}^{-1}$

in narrow-band filters and found that in Mkn 938 [O III] $\lambda 5007$ emission is weak compared to most of the known Seyfert galaxies. In addition, the above authors found that the bright H α emission shows up throughout the entire galaxy. This means that ionization of most of the gas is not associated with any Seyfert activity. Morphologically, the galaxy appears to undergo a merger, as is evidenced by the presence of tidal tails. This conclusion is corroborated by 8.8- and 12.5- μm infrared images of Mkn 938 (Miles et al., 1996), where a binary source with a separation of $1''.2$ was found in the nuclear region of the galaxy. Preliminary results of the integral-field spectroscopy of the central part of this galaxy carried out with the 6-m telescope of the Special Astrophysical Observatory of the Russian Academy of Sciences (Rafanelli et al., 2000) revealed signs of both star formation and gas outflows. In particular, two dynamic centers were found in the NaD line with a separation of $1''$, which coincide with the double source found in the infrared. The extended HI structure found

Send offprint requests to: Victor Afanasiev e-mail: vafan@sao.ru

in the VLA image of this galaxy (Fernández et al., 2010) and the circumnuclear disk found in CO observations performed with ALMA (Xu et al., 2014) suggest that the observed galaxy is a gas-rich interacting system. Deep optical images (Schweizer & Seitzer, 2007) also suggest that Mkn 938 is likely a product of a merger of galaxies with a mass ratio of 1:3. The high IR luminosity indicates that star formation dominates at the center and with a minor contribution from AGN (Gonçalves et al., 1999). This conclusion is confirmed by a detailed study of the infrared spectrum of Mkn 938 (Esquej et al., 2012), which estimates the bolometric contribution of AGN to the total IR luminosity to be 2%. Furthermore, IR images show that star formation occurs within the central 0.5–2 kpc, where merger traces can be seen. However, these authors believe that the presence of an AGN is necessary for explaining the hard X-ray luminosity.

2. OBSERVATIONS

We observed Mkn 938 in the optical with the 6-m telescope of the Special Astrophysical Observatory of the Russian Academy of Sciences (SAO RAS) within the framework of a program of spectrophotometry of Seyfert galaxies. The heliocentric velocity of the center of the galaxy determined from absorption-line spectra (Rothberg & Joseph, 2006) is $5881 \pm 2 \text{ km s}^{-1}$, which implies a distance of 85.2 Mpc for $H_0 = 73 \text{ km s}^{-1} \text{ Mpc}^{-1}$. This corresponds to a sky-plane scale of $395 \text{ pc}''$.

Table 2 presents the log of observations of Mkn 938 at the 6-m telescope: date of observations, total exposure, size of the resulting data cube, seeing, the instrument employed, disperser or filter, spectral range and spectral resolution. A description of the instruments employed (MPFS integral-field spectrograph and focal reducer with a Fabry–Perot interferometer – FPI) can be found in Afanasiev et al. (2001). The data acquired with both instruments was reduced using the technique described in our earlier papers Smirnova et al. (2006); Smirnova & Moiseev (2010).

2.1. Fabry–Perot Interferometer

As a result of observations with a scanning FPI a total of 12 interferograms were acquired that fill sequentially the free spectral interval ($\Delta\lambda \approx 29 \text{ \AA}$ for this interference order). The spectral domain in the neighborhood of redshifted $H\alpha$ line was selected using a narrow-band filter. To reduce readout time and increase the signal-to-noise ratio, TK 1025 1K×1K CCD was read out in the 2×2 instrumental-binning mode. The size of the field of view was 5.8 with a pixel scale of 0.68 pixel^{-1} .

As a result of data reduction we obtained data cube where each pixel in the field of view contains a 12-channel spectrum. We used software Aladin (Boch & Fernique, 2014) for astrometric calibration. We fitted emission lines by Gaussian profiles to construct the brightness distributions in the $H\alpha$ line and the line-of-sight velocity field of

ionized gas shown in Fig. 1. For technical reasons we had to limit our observations to a few interferograms providing a spectrum sampling close to the width of the instrumental contour, and therefore we could not map the distribution of velocity dispersion in the emission line.

The emission line is detected inside the bright stellar disk of the galaxy ($r < 15''\text{--}20''$), and in the emission-line “island” located at a projected distance of $30''\text{--}55''$ Northeast of the nucleus. This “island” is quite conspicuous on broadband Hubble Space Telescope images acquired with the ACS camera and published in Kim et al. (2013), and also on earlier images from Schweizer & Seitzer (2007). Fig. 1 shows an image taken in the F438W blue filter. This emission feature must be a region of intense star formation associated with an extended tidal tail. This is possibly a tidal galaxy with a size of about 6 kpc.

2.2. MPFS integral-field spectrograph

MPFS simultaneously records spectra from 256 spatial elements formed by a $16'' \times 16''$ lens square array placed in the focal plane. In our observations each lens had a size of $1'' \times 1''$. This lens array forms an array of micropupils. Optical fibers reform these micropupils into a pseudoslit at the spectrograph entrance. The sky background spectra are acquired with other fibers located $4'$ from the lens array. The detector was a $2K \times 4.5K$ CCD E2V 42-90. Fig. 1 shows the location of the MPFS array on the galaxy image.

After primary reduction the results had the form of data cubes with a 16×16 element field of view where each element contained a spectrum with bright emission lines typical of Seyfert galaxies— $H\beta$, $[O III] \lambda 4959, 5007$, $H\alpha$, $[N II] \lambda 6548, 6584$ and $[S II] \lambda 6717, 6731$, and absorption lines $H\beta$, $Mg I$ and $Na D$.

To measure the fluxes and radial velocities, we fitted emission lines by Gaussians. A single-component model describes the center of the galaxy far from the line center quite well, however, in the central region ($r < 4''$, see Section 3.2) a second broad component shows up with an amplitude amounting to $\sim 1/4$ of that of the main component. Hereafter we show the velocity fields and flux maps for the main (narrow) component. To take into account the contribution of high-contrast absorptions due to Balmer lines of the stellar population, we fitted the $H\beta$ absorption by another Gaussian. We assumed the velocity and width of the absorption feature in the region of $H\alpha + [N II]$ lines to be the same as in the $H\beta$ neighborhood, and chose the amplitude so as to preserve the same equivalent width of the Balmer lines.

We constructed the velocity field of the stellar population by applying the cross-correlation technique (Moiseev, 2001) using standard spectra of stars in the $5015\text{--}5400 \text{ \AA}$, wavelength interval, which contains high-contrast $Mg I$ and $Fe I$ absorption features. We used the same method to analyze the line-of-sight velocity profiles in the absorp-

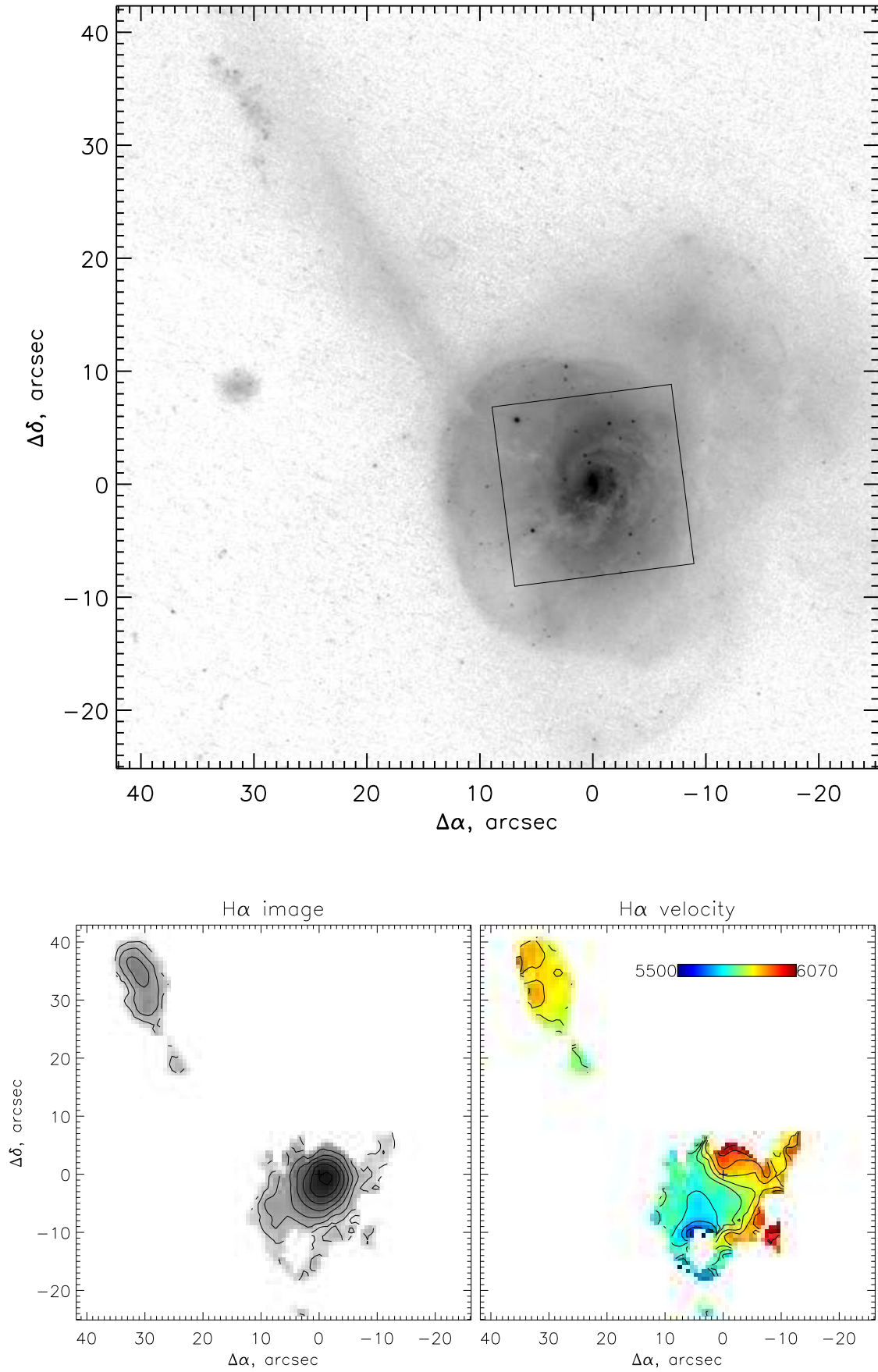
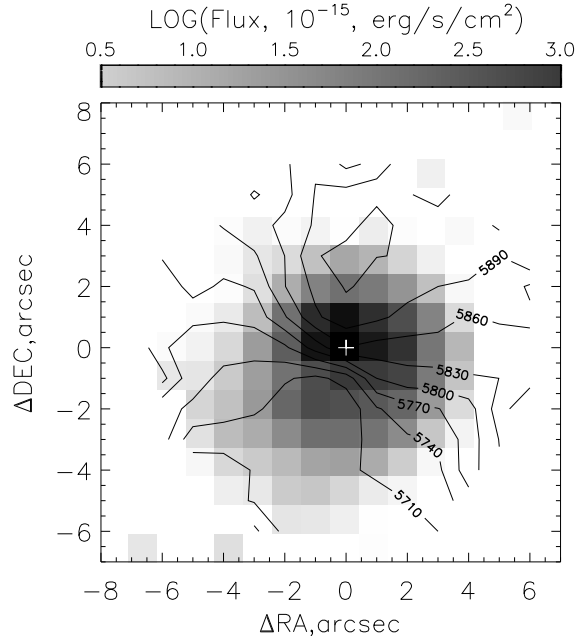


Fig. 1. F435W-band HST image of Mkn 938 obtained with ASC camera (the top panel). The square indicates the field observed with the MPFS. The bottom panels show results of observations made with the scanning FPI: the H α brightness distribution and the velocity field in this line, respectively. The velocity scale is in km s^{-1} . The cross indicates the center of continuum isophotes near H α .

normal

Table 2. Log of observations

Date of observation	Total exp, sec.	Size of data cube	Seeing, arcsec	Device	Disperser or Filter	Spectral coverage, Å	Spectral resolution, Å
1999/12/04	2400	512×512×12	2	focal reducer	FP260	6675–7005	2.5
2009/10/18	9600	16×16×3000	1.5	MPFS	1200/17.7	4790–7740	3

**Fig. 2.** H α velocity field of Mkn 938 superimposed on the V-band continuum image of the central part of the galaxy.

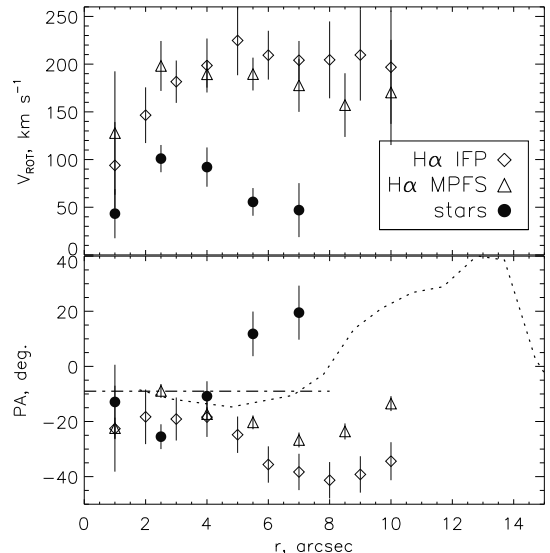
tion line of the Na D, because these radial velocities differ widely from the radial velocities observed both in the stellar population and in ionized gas (see Section 3.2 below). We used night-sky emission lines recorded in the field of view of MPFS as the template Na D spectrum.

3. RESULTS

3.1. Kinematics of Gas and Stars

According to MPFS data, the distribution of radial velocities of ionized gas in the $r < 5''-7''$ agrees, on the whole, with the pattern expected for a flat rotating galactic disk (Fig. 2). This conclusion is also confirmed by FPI observations (Fig. 1) in the H α line. In this region the velocity field is quite consistent with HI radio data (Fernández et al., 2010). However, outside the region observed with the MPFS the velocity field of ionized gas appears significantly different from circular rotation, especially West of the nucleus. At the same time, the radial velocities of the outer emission-line region Northeast of the nucleus (the possible tidal galaxy) agree with the systemic velocity of the center of Mkn 938.

An analysis of the velocity field made by using the tilted-rings method to determine the following parameters in the narrow ring at the given distance r from the

**Fig. 3.** Results of an analysis of the velocity fields of gas and stars: the rotation curves (the top panel) and the position angle of the kinematic major axis (the bottom panel). The dashed line shows the change of orientation of the major axis of the K -band isophotes (Rothberg & Joseph, 2004). The dashed-and-dotted line shows the orientation of the major axis of the inner disk according to Schweizer & Seitzer (2007).

nucleus: rotation velocity V_{rot} , position angle of the kinematic major axis PA_{kin} , inclination i with respect to the line-of-sight, and systemic velocity V_{sys} . A more detailed description of the application of this method to FPI and MPFS data can be found in our earlier papers (Smirnova & Moiseev, 2010; Smirnova et al., 2018). We fixed the inclination at $i = 38^\circ$, in accordance with photometric estimates Rothberg & Joseph (2004) for isophotes of the inner disk in the K band, which is free from dust absorption. We also fixed V_{sys} in accordance with the mean value averaged over the field.

Firstly we determined the position of the kinematic center of rotation based on the assumption that the velocity field is symmetric. In ionized gas (H α measurements with MPFS and FPI) the center of rotation coincides with the center of continuum isophotes. However, in the velocity field of stars the kinematic center is offset North with respect to the photometric center by about $1''$.

Fig. 3 shows the distribution of kinematic parameters along the radius. As is evident from the figure,

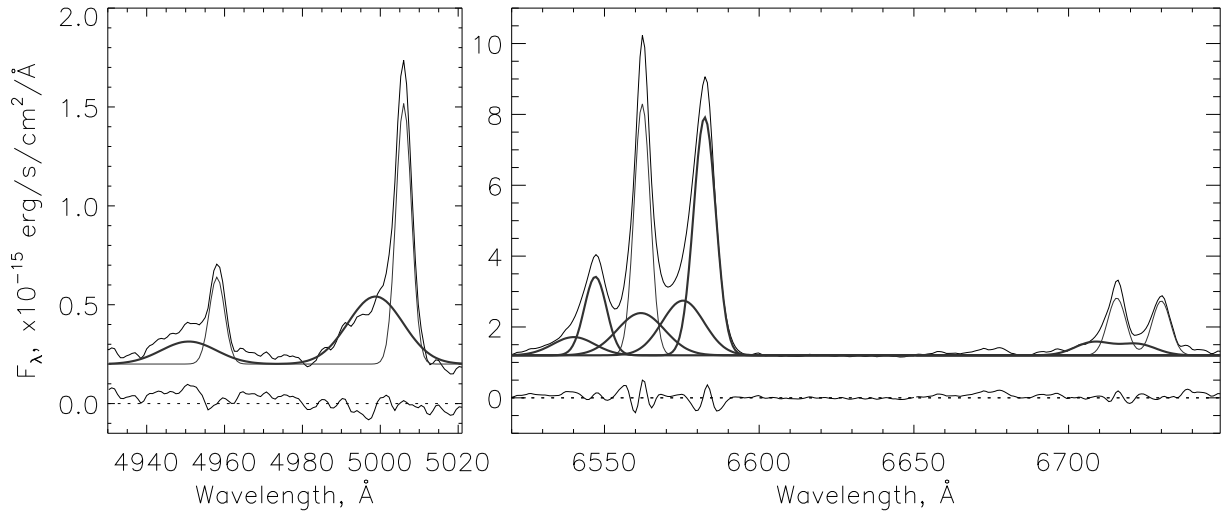


Fig. 4. Integrated rest-frame spectrum of the region where the asymmetry of spectral-line profiles is observed according to MPFS data. Left: emission lines of the [O III] doublet. Right: H α , [N II], and [S II] lines. Also shown is the decomposition of the profiles into the narrow and broad Gaussian components and the residuals obtained after subtracting these components. The spectra are shifted along the vertical axis for convenience.

$PA_{\text{kin}} \approx -20^\circ$ in the inner region, which is close to the available orientation estimates for the inner disk of the galaxy in the optical (Schweizer & Seitzer, 2007) and near IR (Rothberg & Joseph, 2004): $PA_{\text{phot}} \approx -10^\circ$. The small difference between the position angles can be explained by radial mass motions in the circumnuclear spiral structure, which is quite conspicuous in HST images (see Fig. 1). At large distances from the nucleus PA_{kin} in ionized gas begins to strongly deviate from the photometric major axis, which is due either to the increase of noncircular (radial) gas motions or to the warp of the gaseous disk. However, the latter is less likely because the rotation curve at $r = 3''\text{--}10''$ remains practically flat. The parameters of the rotation of stars at $r > 4''$ differ appreciably from this of gas rotation: the kinematic major axis deviates into the opposite direction from the photometric major axis, and the rotation velocity for the adopted i decreases abruptly. Note that in the inner regions V_{rot} for stars is also almost twice smaller than for ionized gas. Such a difference is difficult to explain only by asymmetric drift (higher velocity dispersion) in the stellar disk. Most likely, we see two dynamic subsystems (the main galaxy and the satellite that merges with it) in the stellar velocity field. The superposition of their line-of-sight velocities complicates the observed pattern and makes it impossible to interpret in terms of the model of the circular rotation of a flat disk. At the same time, in the dissipative gaseous system we observe what is already steady quasicircular motion of gaseous clouds.

3.2. Ionized Gas Outflow

According to MPFS data, the profiles of emission lines both in the nucleus and within $r < 4''$ South of

the photometric center show appreciable blue asymmetry. To investigate it with the best signal-to-noise ratio, we coadded the spectra in this region after converting to the rest frame in accordance with the H α velocity field. Fig. 4 shows that the integrated spectrum in each emission line (H α and the [N II] $\lambda 6548, 6583$, [S II] $\lambda 6717, 6731$, [O III] $\lambda 4959, 5007$ doublets) can be described by at least two Gaussian components—a narrow component with width close to instrumental profile FWHM of the spectrograph and another, broader ($FWHM \approx 700\text{--}1000 \text{ km s}^{-1}$) component. Note that the broad component in all forbidden lines is appreciably blueshifted, the relative radial velocities are equal to about $-370, -380, \text{ and } -480 \text{ km s}^{-1}$ in the [N II], [S II], and [O III] lines, respectively.

At the same time, the broad H α component has almost zero velocity relative to the narrow component. Unfortunately, we could not perform a similar analysis for the H β emission because of its low brightness and blending by the stellar H β absorption. However, our data allow us to map the distribution of integrated brightness of [O III] lines and deblended H β emission as shown in Fig. 5. As is evident from the figure, the brightness distributions in the [O III] and H β lines differ appreciably. Whereas brightness maximum in [O III] is located at the center of the galaxy, the corresponding peak of the H β brightness is shifted Westward by $2''$. Isophotes of the H β image have ark-like shape with centers shifted Southwest by $1.5\text{--}2''$. A similar offset is, according to FPI and MPFS data, also observed in the H α line. The average radial velocity determined in the H β absorption is equal to 5890 km s^{-1} , which coincides with the systemic velocity of 5880 km s^{-1} . The narrow H β emission line, on the contrary, is shifted by -200 km s^{-1} .

The observed pattern can be interpreted as wind outflow from the nucleus with velocities of at least

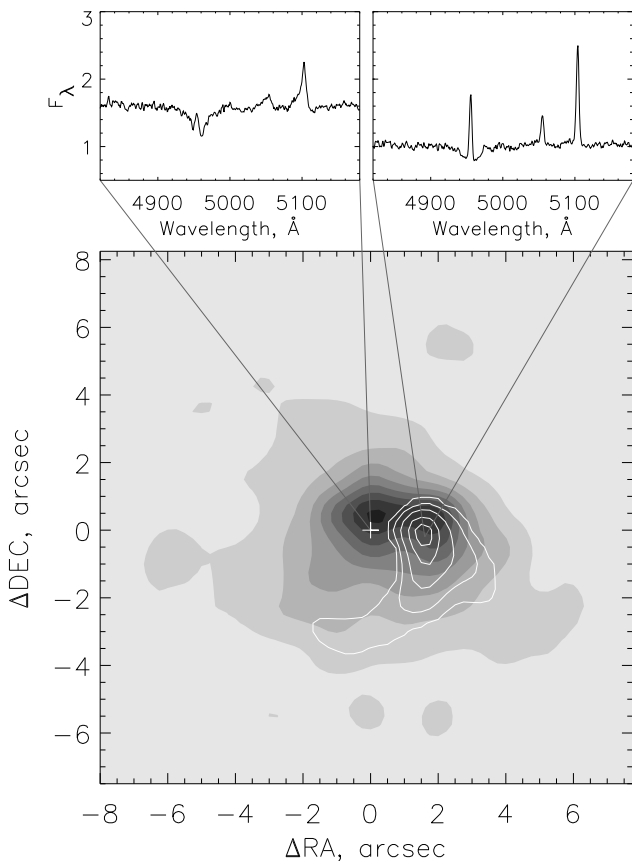


Fig. 5. $H\beta$ emission isophotes superimposed onto the [O III] 5007 image with examples of spectra in the selected regions.

400–500 km s^{-1} , which is often observed in galaxies with powerful starburst. Note that the galactic wind is dominated by shock ionization (Heckman et al., 1990; Westmoquette et al., 2012), as is also evidenced by the shift of the narrow $H\beta$ line. The presence of unshifted broad component in the $H\alpha$ line is indicative of weak nuclear activity and is associated with the broad emission-line region (BLR).

The observed asymmetry can be alternatively explained by the jet-cloud interaction (see Smirnova et al., 2007). However, detailed radio observations with a high spatial resolution revealed no extended structures that could be interpreted as a jet (Fernández et al., 2014).

3.3. Galactic Wind in the Extended Na D Line

The spectrum of the central part of the galaxy exhibits a broad NaD, absorption line blueshifted by 620 km s^{-1} relative to the systemic velocity of 5880 km s^{-1} (Schweizer & Seitzer, 2007). Such lines, which demonstrate high-velocity outflow from the center, are observed in many ultrabright infrared active starburst galaxies (Rupke et al., 2005). We used MPFS data to analyze the variation of observed sodium doublet profiles. Fig. 6 illustrates the idea of our analysis. The cen-

tral panel shows the map of the distribution of equivalent widths of NaD, absorption lines, which we computed in the wavelength interval 5970–6020 Å. The left and right panels show the NaD line profiles and the result of the cross correlation with the NaD lines of the night sky. The velocity scale is printed along the horizontal axis. Negative night-sky line profiles shifted along Z are shown next to the profiles of the object lines. The vertical dashed line indicates the systemic velocity of the galaxy. The cross-correlation curves are actually the profiles of the distribution of NaD radial velocities at the corresponding point of the image. A decomposition of these profiles showed that their shape can be described quite well by two Gaussians of approximately the same width within $FWHM = 600\text{--}900 \text{ km s}^{-1}$. Fig. 7 shows line-of-sight velocity fields for each component. Hereafter we refer to the highly blueshifted feature the high-velocity component and the other one, the low-velocity component. Isophotes in the figure show the distribution of NaD equivalent widths. The high-velocity component at the center has a velocity of -800 km s^{-1} relative to the systemic velocity and its width is of about 700 km s^{-1} , the corresponding parameters of the low-velocity component are -200 km s^{-1} and 900 km s^{-1} , respectively.

4. DISCUSSION

We observe in Mkn 938 the final stage of a merger of two gas-rich galaxies with dominating star formation in the center. Our observations revealed many peculiarities of the stellar and gas kinematics in this galaxy. First, emission-line profiles both in the nucleus proper and within $r < 4''$ South of the photometric center show appreciable blue asymmetry. Whereas in all forbidden lines the broad component is appreciably blueshifted (relative radial velocities range from -370 to -480 km s^{-1} in different lines), the broad component in the $H\alpha$ line has almost zero velocity relative to the systemic velocity. The presence of the unshifted component in the $H\alpha$ line is due to the broad emission-line region (BLR) around the active nucleus of Mkn 938.

The observed pattern can be interpreted as wind outflow with velocities of 400–500 km s^{-1} or higher from the nucleus, as is observed in galaxies with intense star formation. Note that the galactic wind is dominated by shock ionization (Heckman et al., 1990; Westmoquette et al., 2012), which is also evidenced by the shift of the narrow $H\beta$ line. The presence of unshifted broad $H\alpha$ component in the center is indicative of weak activity of the nucleus and is associated with the broad emission-line region (BLR).

The line asymmetry is most likely due to an outflow from the active nucleus. The results of other authors estimating the velocity of gas motion from the center of Mkn 938 based on NaD lines to range from -620 km s^{-1} to -1050 km s^{-1} (Schweizer & Seitzer, 2007) further confirm this hypothesis. Similar outflows can also be observed in starburst galaxies, however outflow velocities in

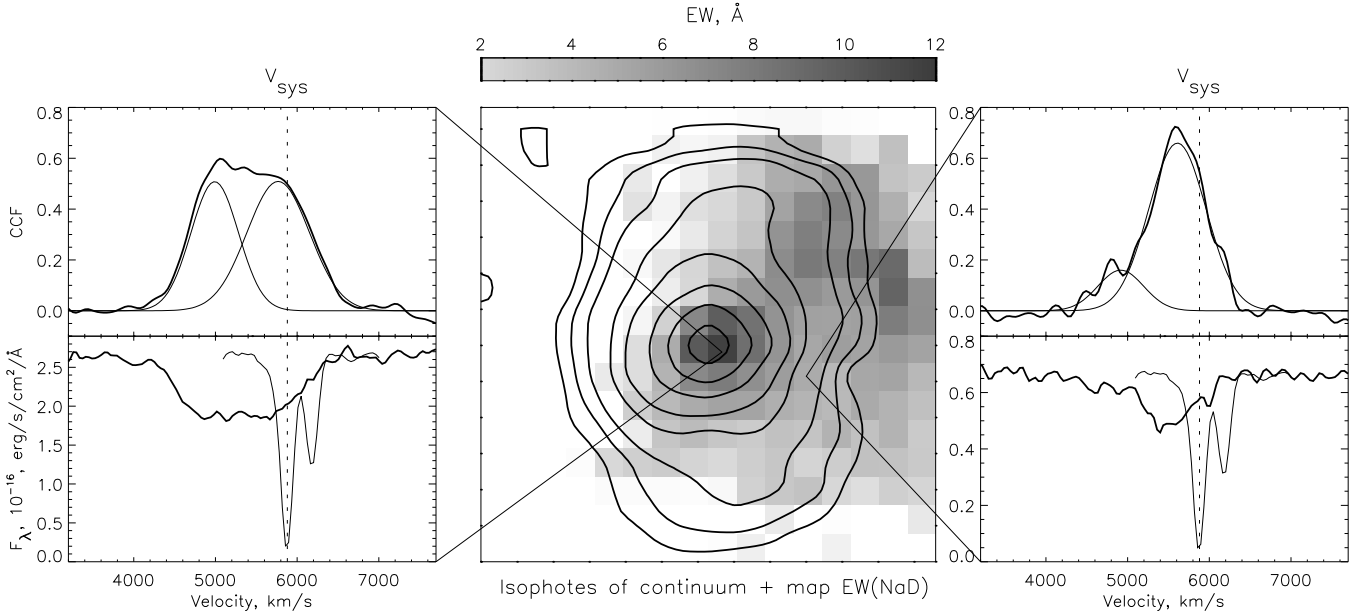


Fig. 6. Map of the distribution of equivalent widths of NaD line with 5500–6300 Å continuum brightness isophotes superimposed and examples of spectra and their analysis in various regions of the image. The thin line shows an invert spectrum of the airglow NaD emission line.

Mkn 938 are too high even for a star-formation rate of $70 \pm 20 M_{\odot} \text{ yr}^{-1}$ (Schweizer & Seitzer, 2007) and can be explained only the influence of the active nucleus. For example, by the presence of a jet, which so far has not been found in radio observations.

High-velocity outflows of neutral gas in the NaD absorption are observed quite often in galactic winds. Such observations are usually made using the long-slit spectroscopy and therefore the spatial structure and extension of the outflows remains unclear. Outflow line-of-sight velocity fields in NaD have so far been constructed only for a few galactic winds (see, e.g., our earlier paper about Mkn 334 (Smirnova & Moiseev, 2010) or a recent study of the wind in NGC 5394 (Martín-Fernández et al., 2016)). Note that the spatial size of the neutral-gas outflow in Mkn 938 is significantly larger, and high-velocity gas is observed out to 3 kpc projected distance from the center. We plan to construct a detailed geometric model of this outflow in a separate paper including new observational data.

We mapped the distributions of the integrated brightness of the [O III] lines and deblended $H\beta$ emission (see Fig. 5). Whereas the [O III] brightness maximum coincides with the continuum image of the galaxy nucleus, the $H\beta$ brightness maximum is offset $2''$ to the West. Note that the $H\beta$ emission is shifted by -200 km s^{-1} relative to the systemic velocity. This effect can be most likely explained by the gas outflow from the nucleus with velocities amounting to $400\text{--}500 \text{ km s}^{-1}$. Gas outflow with a velocity of about 400 km s^{-1} was also discovered in ALMA observations (see Xu et al., 2014).

ALMA observations of Mkn 938 in the CO (6–5) emission line revealed a dynamic structure, which the authors

interpreted as a rotating circumnuclear disk (Xu et al., 2014). However, this disk proves to be highly shifted in velocity terms (the velocity of the disk center is about 5700 km s^{-1}), which is almost 200 km s^{-1} less than the systemic velocity. This shift of the dynamic center can be explained by the fact that what we actually observe in the CO (6–5) line is not a disk but rather an outflow with velocities on the order of 200 km s^{-1} , and the galaxy nucleus then corresponds to velocities of about 5900 km s^{-1} . This systemic velocity agrees well with numerous observations of other authors ($V_{\text{sys}} = 5931 \pm 11 \text{ km s}^{-1}$ —RC3/NED, $5881 \pm 2 \text{ km s}^{-1}$ —Rothberg & Joseph (2006) etc).

5. CONCLUSIONS

We performed a detailed study of the active galaxy Mkn 938 using methods of panoramic spectroscopy. We investigated the peculiarities of the structure of Mkn 938 on different scale lengths, namely:

- At large galactocentric distances ($r > 4''$) the parameters of the rotation of stars differ appreciably from those of gas rotation. The stellar velocity field shows at least two dynamic subsystems: the main galaxy and the nucleus of a companion merging with it, and therefore the superposition of their line-of-sight velocities complicates the observed pattern preventing its interpretation in terms of the model of circular rotation of a flat disk. At the same time, in the gaseous system we observe steady quasi-circular motion of gaseous clouds, which can be used to reconstruct a realistic rotation curve.

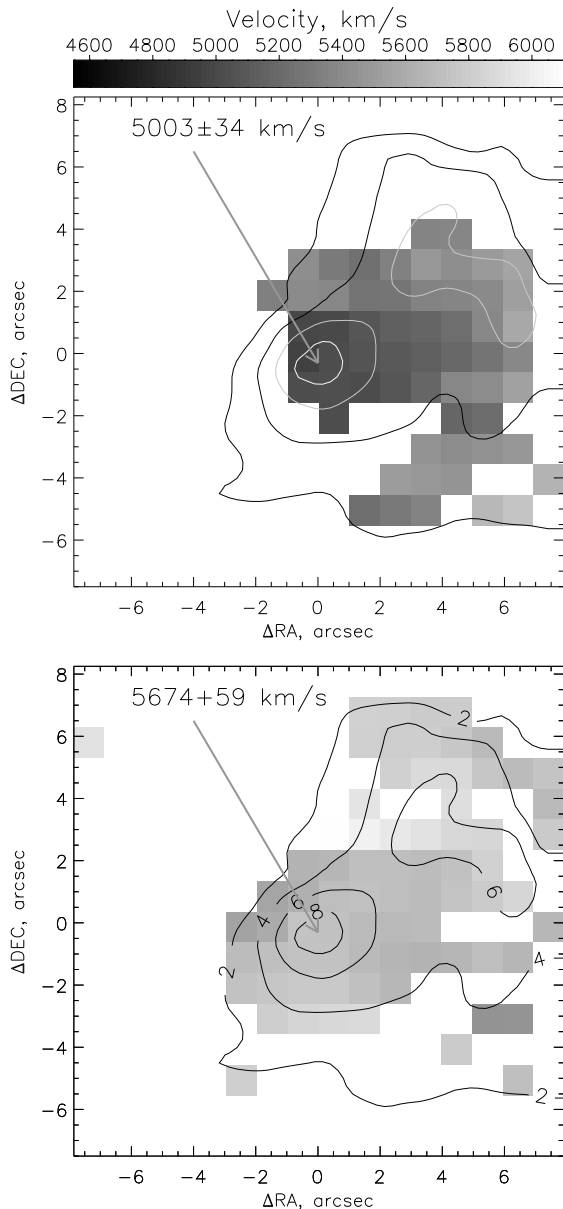


Fig. 7. Velocity field of the high- (the top panel) and low-velocity (the bottom panel) NaD components. The isophotes show the distribution of the equivalent widths of NaD.

- We mapped for the first time in Mkn 938 the galactic wind in the NaD absorption line. A decomposition of the profiles of this line showed that their shape can be described quite well by two Gaussians of about the same width within $FWHM = 600\text{--}900\text{ km s}^{-1}$. We constructed the velocity fields for both, the high- and low-velocity components. The high-velocity component in the center shows a velocity of -800 km s^{-1} relative to the systemic velocity and a width of about 700 km s^{-1} . The corresponding parameters for the low-velocity component are -200 km s^{-1} and 900 km s^{-1} , respectively.

- In the innermost region of the galaxy within $r < 4''$ South of the photometric center a second component blueshifted by up to -500 km s^{-1} is also observed in the emission lines of ionized gas. Furthermore, the brightness center in Balmer lines is appreciably (almost by $2''$ or about 0.8 kpc) offset relative to center of the [O III] and continuum isophotes. All this together can be interpreted either as the ionized component of galactic wind mapped in NaD, or as the effect of the jet emerging from the active nucleus on the interstellar medium. Unfortunately, no jet has so far been detected in radio observations of Mkn 938.

Acknowledgements. We are grateful to the anonymous referee for the comments, which helped to improve the paper. This research has made use of the NASA/IPAC Extragalactic Database (NED), which is operated by the Jet Propulsion Laboratory, California Institute of Technology, under contract with the National Aeronautics and Space Administration. In this paper we present an image from the Hubble Legacy Archive based on observations made with the NASA/ESA Hubble Space Telescope, and obtained from the Hubble Legacy Archive, which is a collaboration between the Space Telescope Science Institute (STScI/NASA), the Space Telescope European Coordinating Facility (ST-ECF/ESA) and the Canadian Astronomy Data Centre (CADC).

FUNDING

This work was supported by the Russian Science Foundation (project No. 17-12-01335 “Ionized gas in galaxy disks and beyond the optical radius”). Observations with the SAO RAS telescopes are supported by the Ministry of Science and Higher Education of the Russian Federation (including agreement No. 05.619.21.0016, project ID RFMEFI61919X0016).

References

- Afanasiev, V. L., Lipovetskii, V. A., Markarian, B. E., & Stepanian, D. A. 1980, *Astrofizika*, 16, 193
- Afanasiev, V. L., Dodonov, S. N., & Moiseev, A. V. 2001, in *Stellar Dynamics: from Classic to Modern*, ed. L. P. Ossipkov & I. I. Nikiforov, 103
- Boch, T. & Fernique, P. 2014, *ASP Conf. Ser.*, 485, 277
- Dahari, O. 1985, *ApJS*, 57, 643
- Esquej, P., Alonso-Herrero, A., Pérez-García, A. M., et al. 2012, *MNRAS*, 423, 185
- Fernández, X., Petric, A. O., Schweizer, F., & van Gorkom, J. H. 2014, *AJ*, 147, 74
- Fernández, X., van Gorkom, J. H., Schweizer, F., & Barnes, J. E. 2010, *AJ*, 140, 1965
- Gonçalves, A. C., Véron-Cetty, M. P., & Véron, P. 1999, *A&AS*, 135, 437
- Heckman, T. M., Armus, L., & Miley, G. K. 1990, *ApJS*, 74, 833
- Kandalyan, R. A. 2003, *A&A*, 398, 493
- Kim, D. C., Evans, A. S., Vavilkin, T., et al. 2013, *ApJ*, 768, 102

- Martín-Fernández, P., Jiménez-Vicente, J., Zurita, A., Mediavilla, E., & Castillo-Morales, Á. 2016, *MNRAS*, 461, 6
- Miles, J. W., Houck, J. R., Hayward, T. L., & Ashby, M. L. N. 1996, *ApJ*, 465, 191
- Moiseev, A. V. 2001, *Bulletin of the Special Astrophysical Observatory*, 51, 11
- Mulchaey, J. S., Wilson, A. S., & Tsvetanov, Z. 1996, *ApJS*, 102, 309
- Osterbrock, D. E. & Dahari, O. 1983, *ApJ*, 273, 478
- Rafanelli, P., Rifatto, A., Afanasiev, V., et al. 2000, in *Astronomical Society of the Pacific Conference Series*, Vol. 195, *Imaging the Universe in Three Dimensions*, ed. W. van Breugel & J. Bland-Hawthorn, 232
- Rothberg, B. & Joseph, R. D. 2004, *AJ*, 128, 2098
- Rothberg, B. & Joseph, R. D. 2006, *AJ*, 131, 185
- Rupke, D. S., Veilleux, S., & Sanders, D. B. 2005, *ApJ*, 632, 751
- Schweizer, F. & Seitzer, P. 2007, *AJ*, 133, 2132
- Smirnova, A. & Moiseev, A. 2010, *MNRAS*, 401, 307
- Smirnova, A. A., Gavrilović, N., Moiseev, A. V., et al. 2007, *MNRAS*, 377, 480
- Smirnova, A. A., Moiseev, A. V., & Afanasiev, V. L. 2006, *Astronomy Letters*, 32, 520
- Smirnova, A. A., Moiseev, A. V., & Dodonov, S. N. 2018, *MNRAS*, 481, 4542
- Veron-Cetty, M. P. & Veron, P. 1986, *A&AS*, 65, 241
- Westmoquette, M. S., Clements, D. L., Bendo, G. J., & Khan, S. A. 2012, *MNRAS*, 424, 416
- Xu, C. K., Cao, C., Lu, N., et al. 2014, *ApJ*, 787, 48